Mixed-mode dynamics and the canard phenomenon: towards a classification

Mixed-mode dynamics and the canard phenomenon: towards a classification

Nikola Popović

University of Edinburgh, School of Mathematics and Maxwell Institute for Mathematical Sciences, James Clerk Maxwell Building, King's Buildings, Mayfield Road, Edinburgh, EH9 3JZ, United Kingdom

E-mail: Nikola.Popovic@ed.ac.uk

Abstract. Mixed-mode dynamics is a complex type of oscillatory behavior that is characterized by an alternation of small-amplitude oscillations and large-amplitude excursions. In this overview article, we focus on one particular mechanism that has been shown to generate mixed-mode oscillations (MMOs) in multiple-scale systems: the generalized canard mechanism. After a brief review of the classical canard phenomenon, we present a model problem that was proposed in [23] as a canonical form for a family of three-dimensional three time-scale systems, and we reiterate some of the results obtained there. In particular, we discuss how that canonical form can be placed in the context of the well-developed geometric theory of canards in three dimensions. Finally, we introduce two examples of problems from mathematical neuroscience that fit into the framework of our model problem, and we discuss the implications of our results for the mixed-mode dynamics observed in these two examples. Our results are intended as a first step towards a more general classification of the mixed-mode dynamics that can arise via the generalized canard mechanism, with the long-term goal of constructing a 'toolbox' of prototypical minimal models.

1. Introduction

Mixed-mode oscillatory dynamics is characterized by time series in which small-amplitude (sub-threshold) oscillations alternate with large-amplitude (relaxation-type) excursions. Mixed-mode behavior is abundant in applications and occurs in a variety of disciplines, from chemical kinetics, where MMOs were first described in the famous Belousov-Zhabotinsky reaction [45], to electrocardiac dynamics, neuronal modeling and laser dynamics, to name but a few examples [11, 20, 24, 30, 31, 34, 36, 37, 38].

Mixed-mode oscillations (MMOs) are frequently found in multiple-scale systems of ordinary differential equations, i.e., in systems in which the dynamics evolves on two (or more) fundamentally different scales. While a number of mechanisms have been proposed to explain mixed-mode dynamics, see e.g. [15, 16, 20, 28, 29], no unified approach seems to have been developed thus far. In this overview article, we focus on the so-called *generalized canard mechanism* that has recently been suggested in the context of three-dimensional systems of singularly perturbed ordinary differential equations. This approach, which was originally brought forward by Milik *et al.* in their analysis of the autocatalator [33], has since been extended and refined by a number of authors, including Brøns, Krupa and Wechselberger [4], Krupa, Popović and Kopell [23], and Krupa and Wechselberger [27]. In essence, the generalized

canard mechanism is defined as a combination of local passage through a so-called *canard point* and an appropriately formulated global return mechanism that resets the dynamics after the local passage has been completed. As was noted in [33], the precise nature of the mixed-mode dynamics observed in a given problem—and, in particular, the structure of the specific mixed-mode patterns that can occur—will depend on the interplay of those two aspects (local and global).

Canard phenomena have been analyzed by a number of authors using a wide array of analytic methods, both standard and non-standard; relevant references include [1, 3, 9, 10, 32, 33, 40, 41, 43], among many others. For the purposes of this article, we will focus on the geometric approach that was pioneered by Dumortier and Roussarie in their analysis of canard cycles in [9] and that was later extended by Krupa and Szmolyan in [25]; see also [41] and the references therein. That approach, which is widely known as '*blow-up*,' or *(geometric) desingularization*, builds on geometric singular perturbation theory and has been applied successfully in the study of numerous situations where a loss of normal hyperbolicity occurs. In particular, it underlies the analysis of mixed-mode dynamics via the generalized canard mechanism in [4, 23, 24, 43].

One of our goals in this article is to illustrate a particular realization of that very broad mechanism. To that end, we discuss in some detail one specific family of three-dimensional fast-slow systems that exhibits mixed-mode dynamics upon variation of a control parameter. This family, which was studied in [23], is characterized by the fact that its dynamics evolves on three distinct time-scales. The 'near-integrability' that results from this three time-scale structure allows for a fairly explicit analysis: by combining a leading-order approximation of the global return with detailed local asymptotics about the underlying canard point, we obtained a precise description of the return map induced by the flow of the equations. In a second step, that map was further reduced, in an exponentially accurate fashion, to a one-dimensional map. This additional reduction allowed us to characterize the dynamics of the system in considerable detail; in particular, we found that the structure of the resulting mixed-mode sequences is determined by the presence of bifurcating ('secondary') canards, and we were able to derive (asymptotic) estimates on the relevant parameter regimes. An in-depth discussion of our results can be found in [23].

Finally, we note that the analysis in [23] was intended as one part of a more ambitious program to establish a general classification of the mixed-mode dynamics that is possible in three-dimensional fast-slow systems, as well as to provide an associated 'toolbox' of canonical (normal form) equations for the various types of dynamics. Comparable results had previously only been obtained by Wechselberger [43], who performed an analysis similar to ours for a different realization of the generalized canard mechanism, classifying the mixed-mode dynamics therein. In that sense, our work in [23] can be regarded as a complement to [43]; see also [4] for a related discussion.

This article is organized as follows: in Section 2, we give a brief overview of the canard phenomenon, both in two and in three dimensions; we then focus on the latter case, continuing with a classification of folded singularities and their potential for generating mixed-mode dynamics in Section 3. Then, in Section 4, we introduce a family of equations that was first proposed in [23] as a canonical form for a family of three-dimensional three time-scale systems. In Section 5, we present the Wilson-Callaway model for the dopaminergic neuron in rats and a modification of the classical Hodgkin-Huxley equations as two example problems that can be reduced to that canonical form; its dynamics is revisited in more detail in Section 6, where we detail how the return map induced by the corresponding flow can be approximated using geometric singular perturbation theory and blow-up. Finally, in Section 7, we conclude with a discussion of our results and an outlook at future research.

2. The canard phenomenon

In this section, we review the notion of canards, beginning with the traditional two-dimensional setting. We then focus on canards in three dimensions, which is the case that is of most interest to us here.

2.1. Canards in $\mathbb{R}^2$

The classical *canard phenomenon* [1, 3, 9, 10, 32] was first identified in two-dimensional systems of fast-slow type, i.e., in planar systems with one fast and one slow variable in the standard form

$$\varepsilon \dot{x} = f(x, y, \lambda, \varepsilon), \tag{1a}$$
$$\dot{y} = g(x, y, \lambda, \varepsilon), \tag{1b}$$

where $0 < \varepsilon \ll 1$ is the perturbation parameter, the overdot stands for differentiation with respect to time τ, and λ denotes the (small) *canard parameter*. A prototypical example in this context is given by the system

$$\varepsilon \dot{x} = -y + f_2 x^2 + f_3 x^3, \tag{2a}$$
$$\dot{y} = x - \lambda, \tag{2b}$$

with both $f_2 > 0$ and $f_3 < 0$ real and constant. Clearly, (2) is singularly perturbed, with x fast and y slow. The corresponding *critical manifold*, which we denote by $\mathcal{S}_0$, is obtained by setting $\varepsilon = 0$ in (2). We note that $\mathcal{S}_0$ is S-shaped and that it can be parametrized by x, i.e., $\mathcal{S}_0 = \big\{(x, y) \in \mathbb{R} \times \mathbb{R} \,\big|\, f(x, y, 0) = 0\big\}$, where $y = \phi(x) := f_2 x^2 + f_3 x^3$; see Figure 1. Moreover, $\mathcal{S}_0$ is normally hyperbolic away from the *fold points* ('knees') at $x^- = 0$ and $x^+ = -\frac{2}{3}\frac{f_2}{f_3}$ and can thus be written as the union of two normally attracting branches $\mathcal{S}_0^{a-}$ and $\mathcal{S}_0^{a+}$ and a normally repelling branch $\mathcal{S}_0^r$.

From geometric singular perturbation (Fenichel) theory [12, 19], it follows that normally hyperbolic segments of $\mathcal{S}_0$ will perturb smoothly to nearby segments of a *slow manifold* $\mathcal{S}_\varepsilon$. (We will denote the segments corresponding to $\mathcal{S}_0^{a\mp}$ and $\mathcal{S}_0^r$ by $\mathcal{S}_\varepsilon^{a\mp}$ and $\mathcal{S}_\varepsilon^r$, respectively.) At the two fold points, however, normal hyperbolicity breaks down. Projecting the *reduced flow* that is obtained for $\varepsilon = 0$ in (2) onto x-space near x^- by differentiating the approximate constraint $y \approx f_2 x^2$, we find $2 f_2 \dot{x} \approx x - \lambda$. Generically, that reduced equation is singular at the origin, which leads to blow-up of solutions there. Trajectories typically leave $\mathcal{S}_\varepsilon$ at such points subject to the fast flow of (2), resulting e.g. in relaxation dynamics [32, 42].

Alternatively, a loss of normal hyperbolicity can give rise to canard dynamics: only in the degenerate case when $\lambda = 0$ can the reduced flow cross the fold in finite time. The origin is called a *canard point* in that case. In the context of (2), the term *canard explosion* [26] denotes a transition from a stable equilibrium through a family of small-amplitude limit cycles and subsequently to a large-amplitude relaxation oscillation as λ passes through zero; cf. Figure 1 for an illustration. In particular, the onset of the small-amplitude regime is marked by a Hopf bifurcation; canard solutions are trajectories that can stay close to the repelling branch $\mathcal{S}_\varepsilon^r$ of $\mathcal{S}_\varepsilon$ for a considerable amount of time before being attracted to either $\mathcal{S}_\varepsilon^{a-}$ or $\mathcal{S}_\varepsilon^{a+}$. The corresponding canard trajectories are known as 'headless canards' and 'canards with head,' respectively; see Figures 1(b) and 1(c). A *maximal canard* is a canard trajectory that follows $\mathcal{S}_\varepsilon^r$ until it reaches the upper fold at x^+. Finally, it is important to note that this two-dimensional canard phenomenon is highly sensitive: the canard explosion in (2) unfolds over an exponentially small (in ε) λ-interval and is hence only rarely observed in applications. (Rather, the influence of noise typically results in a 'hard' transition, in that the amplitude of the oscillation changes abruptly from $\mathcal{O}(\sqrt{\varepsilon})$ to $\mathcal{O}(1)$.)

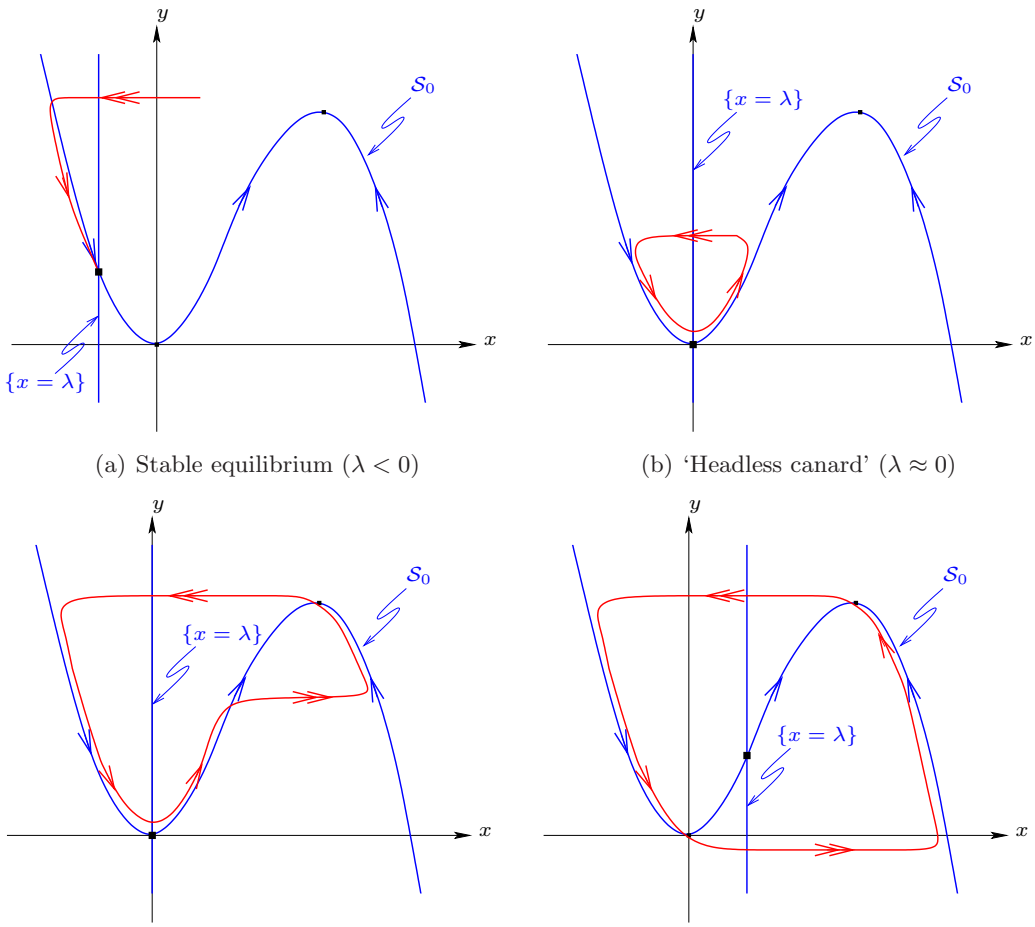

(a) Stable equilibrium ($\lambda < 0$)

(b) 'Headless canard' ($\lambda \approx 0$)

(c) 'Canard with head' ($\lambda \approx 0$)

(d) Relaxation oscillation ($\lambda < 0$)

Figure 1. Nullcline movement leading to a canard explosion in (2).

2.2. Canards in $\mathbb{R}^3$

It is, by contrast, well-known that the canard phenomenon is generic and robust in three dimensions (or, alternatively, in higher-dimensional problems whose dimension can be reduced to three), in the sense that the relevant parameter intervals are 'relatively large.'

Without loss of generality, we will in the following consider the family of three-dimensional systems

$$\varepsilon \dot{x} = f(x, y, z, \varepsilon), \tag{3a}$$
$$\dot{y} = g_1(x, y, z, \varepsilon), \tag{3b}$$
$$\dot{z} = g_2(x, y, z, \varepsilon), \tag{3c}$$

i.e., systems in standard form with one fast variable (x) and two slow variables (y and z). Here, f, g_1 and g_2 are assumed to be sufficiently smooth functions in all of their arguments, and ε is again the small parameter. (Note that in contrast to (1), there is no explicit dependence on an additional parameter λ in (3).)

For the purposes of this review, we make a number of specific assumptions on the geometry of (3): in analogy to the two-dimensional case discussed in the previous subsection, we assume that the critical manifold $\mathcal{S}_0 = \left\{(x, y, z) \in \mathbb{R} \times \mathbb{R}^2 \,\middle|\, f(x, y, z, 0) = 0\right\}$ is a two-dimensional,

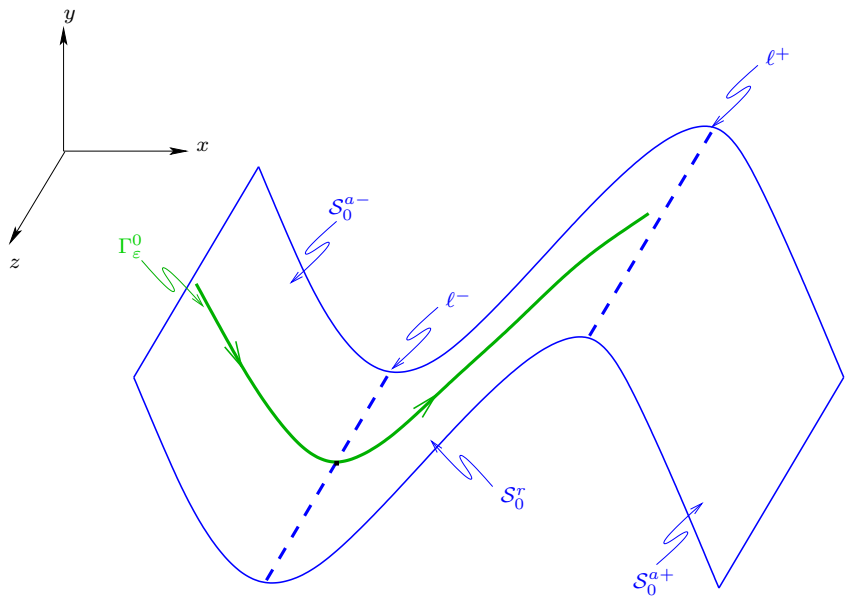

Figure 2. Geometry of the three-dimensional system (3).

S-shaped surface in $\mathbb{R}^3$ that consists of two normally attracting sheets $\mathcal{S}_0^{a-}$ and $\mathcal{S}_0^{a+}$ and a normally repelling sheet $\mathcal{S}_0^r$. These sheets are separated by two fold curves, which we label ℓ^- and ℓ^+; the resulting geometry is illustrated in Figure 2. As before, it follows from standard geometric theory [12, 19] that $\mathcal{S}_0$ will persist, for $\varepsilon > 0$ sufficiently small, as a locally invariant slow manifold $\mathcal{S}_\varepsilon$ away from the fold curves $\ell^\mp$.

Additionally, following [25], we assume that $\mathcal{S}_0$ is a non-degenerate folded surface close to the origin. (Sufficient conditions to that end are given by $f(0,0,0,0) = 0$, $f_x(0,0,0,0) = 0$, $f_y(0,0,0,0) \neq 0$ and $f_{xx}(0,0,0,0) \neq 0$, which imply that $\mathcal{S}_0$ is approximately a parabolic cylinder.) Finally, assuming that the fold curve ℓ^- in (3) can be parametrized by z, we can write $\mathcal{S}_0$ locally as the graph of a function of x and z.

Under the above assumptions, we have $\mathcal{S}_0 = \mathcal{S}_0^{a-} \cup \ell^- \cup \mathcal{S}_0^r$ in a neighborhood of the origin. The so-called *reduced system* [41] projected onto the (x,z)-plane is then given by

$$-f_x\dot{x} = f_y\dot{y} + f_z\dot{z}, \tag{4a}$$
$$\dot{z} = g_2, \tag{4b}$$

which is singular at ℓ^-, i.e., for $x = 0$. Hence, standard existence and uniqueness results do not hold there; in particular, different solutions can approach the same point on ℓ^- in finite time. The equations in (4) can be desingularized by a rescaling of time:

$$\dot{x} = f_y g_1 + f_z g_2, \tag{5a}$$
$$\dot{z} = -f_x g_2. \tag{5b}$$

(This rescaling, which corresponds to a multiplication of the right-hand sides in (4) by a factor of $-f_x$, removes the singularity at points where $f_x = 0$; however, it reverses the orientation of orbits on the repelling sheet $\mathcal{S}_0^r$, since $f_x > 0$ there.)

The dynamics of (3) at the fold depends fundamentally on the properties of the reduced system (5): points on ℓ^- at which the so-called *normal switching condition* (or transversality condition) $(f_y, f_z) \cdot (g_1, g_2)|_{\ell^-} \neq 0$ [32] is satisfied are called *jump points*. Since the reduced

flow is directed towards the fold (or away from it) at such points, solutions have to exit into relaxation ('jump') after reaching ℓ^-, giving rise to relaxation dynamics [42].

Equilibria of (5), on the other hand, are points on ℓ^- at which the normal switching condition is violated. (Alternatively, these points are characterized by the fact that the projection of the reduced flow onto the (y, z)-plane is tangent to the fold curve at the origin.) It is important to note that equilibria of (5), which are known as *folded equilibria*, are not typically equilibria of (4). However, these points are of crucial importance for understanding the canard phenomenon in the context of (3), since it is there that the reduced flow can cross from the attracting sheet $\mathcal{S}_\varepsilon^{a-}$ of the slow manifold to the repelling sheet $\mathcal{S}_\varepsilon^r$. That crossing property is a prerequisite for the existence of canards.

In analogy to the two-dimensional case, the *strong canard* Γ_ε^0 is now defined as a canard trajectory that exists in the intersection of $\mathcal{S}_\varepsilon^{a-}$ with $\mathcal{S}_\varepsilon^r$ and that stays close to $\mathcal{S}_\varepsilon^r$ until it reaches the 'upper' fold curve ℓ^+; see again Figure 2.

In addition to being robust in three dimensions, canard trajectories typically act as separatrices, organizing the dynamics in phase space. In systems of the form (3) that exhibit mixed-mode behavior, for example, the strong canard marks the boundary between small-amplitude (sub-threshold) oscillations and large-amplitude (relaxation-type) excursions. This observation was first made in [33] and later elaborated on in [43] as well as in [23]. Additionally, canards have been linked to delay effects, delaying e.g. the onset of firing in neurons [43], as well as to chaotic dynamics, such as in the case of the van der Pol oscillator with periodic forcing [43].

3. Folded equilibria classified

In this section, we provide an overview of how the equilibria of (5) can be classified. We then discuss the implications of that classification with regard to the potential for mixed-mode dynamics in (3). Most of the following discussion is based on work by Krupa, Szmolyan and Wechselberger; see [4, 41, 43] for a partial list of references.

As was shown e.g. in [41], the fast-slow system (3) in standard form can be transformed, via a sequence of affine transformations, to the normal form

$$\varepsilon \dot{x} = -y + x^2 + \ldots, \tag{6a}$$
$$\dot{y} = x - \alpha z + \ldots, \tag{6b}$$
$$\dot{z} = \beta + \ldots; \tag{6c}$$

here and in the following, dots denote higher-order terms in x, y, z and ε. Hence, the desingularized, rescaled system corresponding to (5) simplifies to

$$\dot{x} = -x + \alpha z + \ldots, \tag{7a}$$
$$\dot{z} = -2\beta x + \ldots. \tag{7b}$$

Folded equilibria of (6) can now easily be classified by classifying the equilibria of the planar system (7): assume that the origin is one such (isolated) equilibrium, let λ_j $(j = 1, 2)$ denote the eigenvalues of the corresponding linearization, and let $\mu = \frac{\lambda_2}{\lambda_1}$ be the ratio of these eigenvalues.

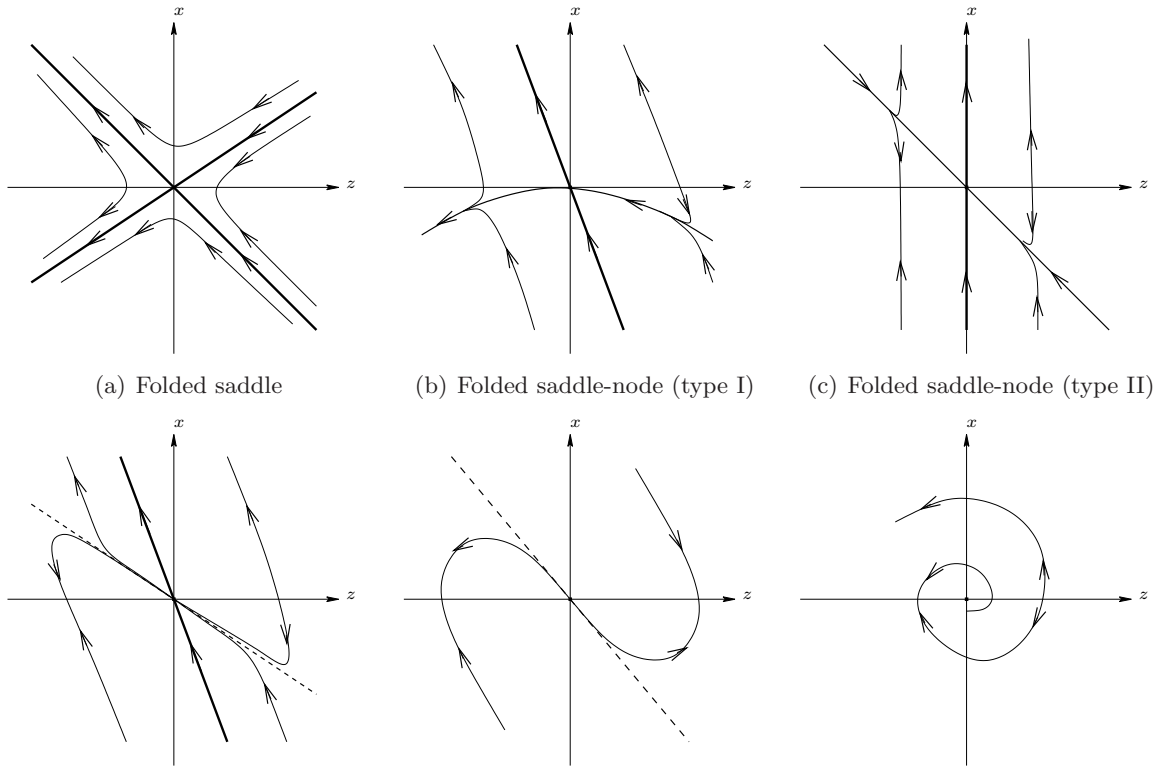

(a) Folded saddle (b) Folded saddle-node (type I) (c) Folded saddle-node (type II)

(d) Folded node (e) Degenerate folded node (f) Folded focus

Figure 3. Classification of folded equilibria in (6).

Then, we have the following classification of the origin in dependence on α and β in (7):

$$\alpha\beta < 0 : \text{folded saddle } (\lambda_1 < 0 < \lambda_2) \tag{8a}$$

$$\alpha\beta = 0 : \text{folded saddle-node } (\lambda_1 < 0 = \lambda_2) \tag{8b}$$

$$0 < \alpha\beta < \frac{1}{8} : \text{folded node } (\lambda_1 < \lambda_2 < 0) \tag{8c}$$

$$\alpha\beta = \frac{1}{8} : \text{degenerate folded node } (\lambda_1 = \lambda_2 < 0) \tag{8d}$$

$$\alpha\beta > \frac{1}{8} : \text{folded focus } (\Re(\lambda_1), \Re(\lambda_2) < 0). \tag{8e}$$

A schematic illustration of the local phase portraits for (7) corresponding to the classification in (8) is given in Figure 3: unique canard solutions are shown in bold, while dashed lines correspond to tangent directions of non-unique solutions, see [41] for details.

We first consider the case where the origin in (3) is a folded saddle, cf. (8a) and Figure 3(a). Then, there exists a unique canard solution connecting $\mathcal{S}_\varepsilon^{a-}$ to $\mathcal{S}_\varepsilon^r$, see [1] as well as [41]. Since no mixed-mode dynamics is possible [27], we will disregard that case in the following. Similarly, since the folded foci in (8e) support no canard solutions, they are of no interest to us and will not be discussed further here. Hence, we now focus on the remaining cases in (8), those of the folded saddle-node and the folded node.

3.1. Folded saddle-nodes

Since $\alpha\beta = 0$ must hold for a folded saddle-node singularity to be present in (3), there are two possibilities in that case. These will be discussed separately below; an in-depth geometric

analysis of the folded saddle-node will be provided in [27]. For the purposes of our discussion, it is important to note that both types of folded saddle-node allow for non-trivial mixed-mode dynamics.

3.1.1. Type I: $\alpha \to 0$ For $\alpha \to 0$ in (8b), the folded equilibrium at the origin in (3) is a *folded saddle-node of type I*; the center manifold corresponding to the zero eigenvalue is tangent to the fold curve ℓ^- in that case, see Figure 3(b). The resulting canonical form is given by

$$\varepsilon \dot{x} = -y + x^2 + \ldots, \tag{9a}$$

$$\dot{y} = (\mu + 1)x - \frac{\mu}{2}z + \ldots, \tag{9b}$$

$$\dot{z} = 1 + \ldots, \tag{9c}$$

where $\mu = \frac{\lambda_2}{\lambda_1}$, as before.

At $\mu = 0$, the equations in (9) undergo a (true) saddle-node bifurcation of folded equilibria; more specifically, a folded saddle and a folded node coalesce into a folded saddle-node before disappearing altogether. The (local) phase portrait depends substantially on the higher-order terms in (9); see [27] for details.

3.1.2. Type II: $\beta \to 0$ In this case, with $\beta \to 0$ in (8b), the center manifold is transverse to ℓ^-, as shown in Figure 3(c), which gives the canonical form

$$\varepsilon \dot{x} = -y + x^2 + \ldots, \tag{10a}$$

$$\dot{y} = (\mu + 1)x - z + \ldots, \tag{10b}$$

$$\dot{z} = \frac{\mu}{2} + \ldots. \tag{10c}$$

(The flow on that center manifold again depends on the higher-order terms in (10).) In contrast to (9), the type II-equations now have a folded singularity at the origin for all values of μ. That singularity is a folded saddle for $\mu < 0$ and a folded node for $\mu > 0$. Hence, the system undergoes a transcritical bifurcation at $\mu = 0$, where an interchange of type of singularity (regular and folded) occurs. Moreover, this *folded saddle-node of type II* involves slow passage through a Hopf bifurcation [13] as well as a delayed loss of stability after desingularization; see again [27].

3.2. (Degenerate) folded nodes

The folded node case with $0 < \alpha\beta \leq \frac{1}{8}$ is well-studied [14, 41, 43]; cf. (8c) and (8d) as well as Figures 3(d) and 3(e). Indeed, it was shown e.g. by Wechselberger [43] that there exists a unique strong canard and a non-unique weak canard in that case. Additionally, there is a finite number of secondary canards; these new canard solutions bifurcate from the weak canard at odd ('resonant') integer values of the parameter μ. As was illustrated numerically in [43] as well as in more detail in [6], the resulting family of canards (primary and secondary) forms a trapping region ('*funnel*') at the fold, which delays solutions in their passage near the singularity. The delay is due to the rotational properties of the manifolds $\mathcal{S}_\varepsilon^{a-}$ and $\mathcal{S}_\varepsilon^{r}$ in the fold region, see again [6]. Mixed-mode dynamics is possible, and has indeed been observed in a number of applications where a folded node singularity is present [7, 38]. Finally, in contrast to the folded saddle-node case, only the leading-order terms in (6) have to be considered in the analysis.

4. A canonical model

While the (local) canard dynamics near a folded node as well as the resulting mixed-mode behavior are well-understood, see [43], no comparable results seem to be available thus far

in the rather more involved folded saddle-node scenario. However, it is possible to paint a fairly complete picture of the dynamics in a related case, which, in the context of the above classification, could be defined as a 'folded saddle-node of type II with weak global return.' Here, the difference from a regular folded saddle-node is due to the fact that the z-variable varies on a third, 'super-slow' time-scale, which substantially simplifies the analysis. To be precise, we now consider the family of three-dimensional three time-scale systems

$$\varepsilon\dot{x} = -y + f_2x^2 + f_3x^3, \tag{11a}$$
$$\dot{y} = x - z, \tag{11b}$$
$$\dot{z} = \varepsilon(\mu + \dots), \tag{11c}$$

where $f_2 > 0$ and $f_3 < 0$ are constants, and the free parameter μ has been explicitly rescaled by ε to reflect its smallness. We note that although the theory of singularly perturbed systems is only well-developed for the classical case of two time-scales, the dynamics of (11) can still be described in considerable detail. As will become clear through our discussion, the reason is the 'near-integrability' of (11) in the fold region, as well as the fact that no slow passage through a Hopf bifurcation occurs, in contrast to the regular folded saddle-node case. These two aspects combined allow for a relatively explicit analysis.

5. Two examples

In this section, we briefly discuss two examples of problems that can be shown to fall into the three time-scale framework of (11). Both of these problems derive from mathematical neuroscience, and both can be reduced explicitly (via a center manifold reduction) to the canonical form in (11). In fact, the first example below served as our original motivation for formulating that canonical form; for details, see [23, 24] as well as the upcoming article [21].

5.1. The Wilson-Callaway model

In [44], Wilson and Callaway introduced an N-compartment model of electrically coupled oscillators to model the oscillation mechanism of the dopaminergic neuron in rats,

$$\dot{v}_i = \frac{1}{C}\big[g_{\mathrm{Ca}}(v_i)(E_{\mathrm{Ca}} - v_i) + g_{\mathrm{KCa}}(u_i)(E_{\mathrm{K}} - v_i) + g_\ell(E_\ell - v_i) + G_i(v_{i+1} - 2v_i + v_{i-1})\big], \tag{12a}$$
$$\dot{u}_i = \frac{4\beta}{d_i}\Big[\frac{1}{zF}g_{\mathrm{Ca}}(v_i)(E_{\mathrm{Ca}} - v_i) - P_{\max}u_i\Big]; \tag{12b}$$

here, v_i, u_i and G_i ($i = 1, \dots, N$) denote the membrane potential, calcium concentration and conductivity in the ith compartment, respectively, C is the capacitance, and d_i denotes the diameter of the ith compartment. The first three terms in (12a) stand for intrinsic currents: a voltage-gated calcium current, a calcium-gated potassium current and a leak current. The fourth term models the diffusive coupling between compartments, while the second term in (12b) represents calcium efflux from the compartment.

The equations in (12) display a variety of oscillatory patterns that change with coupling strength; some of these patterns include rhythmic single spiking, irregular firing and bursting [44]. As was shown in [44], that oscillation mechanism is due to the calcium and potassium currents in (12). In particular, the voltage-gated calcium current represented by the term $g_{\mathrm{Ca}}(v_i)(E_{\mathrm{Ca}} - v_i)$ is essential: if too much calcium is removed from the system, the mechanism breaks down. Here, it is important to note that the oscillation frequency of each compartment is determined by its surface-to-volume ratio and that the frequency of more distal compartments increases, since the diameter d_i decreases.

These observations led Medvedev and Cisternas [31] to introduce a simplified model system for (12), wherein they considered only the two-compartment case:

$$\varepsilon \dot{v}_1 = a(E_2 - v_1)[f(v_1) - u_1] + d(v_2 - v_1), \tag{13a}$$

$$\dot{u}_1 = \omega_1 \big[g_1(v_1)(E_1 - v_1) - \frac{u_1}{\tau} \big], \tag{13b}$$

$$\dot{v}_2 = a(E_2 - v_2)[f(v_2) - u_2] + d(v_1 - v_2), \tag{13c}$$

$$\dot{u}_2 = \omega_2 \big[g_1(v_2)(E_1 - v_2) - \frac{u_2}{\tau} \big]. \tag{13d}$$

Here,

$$f(v) = \frac{g_1(v)(E_1 - v) + \bar{g}_3(E_3 - v)}{a(E_2 - v)} + \frac{b}{a}$$

is a qualitatively cubic function, the coupling is symmetric with coupling strength d, and τ corresponds physiologically to the rate of calcium efflux. Moreover, ω_1 and ω_2 denote the intrinsic frequencies of the somatic and the dendritic compartment, respectively.

Clearly, (13) is a fast-slow system, since the singular perturbation parameter ε is assumed to be small. An additional scale is introduced by the assumption that $\omega_1 \ll \omega_2$: since the neuron is tapering, the diameter of the dendritic (2-)compartment is much smaller than that of the somatic (1-)compartment. It then follows that the dynamics of (13) evolves on three distinct time-scales.

The analysis in [31] was restricted to the case of strong coupling, with $d \gg 1$. The relevant bifurcation parameter in that case is given by τ: as τ is increased, the firing of the neuron is delayed, and the firing patterns become increasingly irregular. Some exemplary firing sequences are displayed in Figure 4. We observe the unfolding of an entire family of MMOs: starting with the relaxation regime in Figure 4(a), the dynamics passes through a series of mixed-mode sequences in Figures 4(b) through 4(e) until, for τ sufficiently large, the sub-threshold regime is reached in Figure 4(f). (Here, we have introduced the following symbolic notation: let $L_j^{k_j}$ denote the orbit segment that consists of L_j relaxation excursions followed by k_j small-amplitude oscillations. To any mixed-mode orbit, one can then assign a *Farey sequence* $\{L_j^{k_j}\}_{j \geq 1}$ [18] of such symbols. In particular, the sequences $\{L^0\}$ and $\{0^k\}$ correspond to the relaxation and the sub-threshold regime, respectively.)

5.2. The Hodgkin-Huxley equations

Our second example concerns a modification of the classical Hodgkin-Huxley equations for the squid giant axon [17] that is due to Doi, Nabetani and Kumagai [8]:

$$\dot{v} = \frac{1}{C} \big[I - g_{\mathrm{Na}} m^3 h (v - E_{\mathrm{Na}}) - g_{\mathrm{K}} n^4 (v - E_{\mathrm{K}}) - g_\ell (v - E_\ell) \big], \tag{14a}$$

$$\dot{m} = \frac{1}{\tau_m} \big[\alpha_m(v)(1 - m) - \beta_m(v) m \big], \tag{14b}$$

$$\dot{h} = \frac{1}{\tau_h} \big[\alpha_h(v)(1 - h) - \beta_h(v) h \big], \tag{14c}$$

$$\dot{n} = \frac{1}{\tau_n} \big[\alpha_n(v)(1 - n) - \beta_n(v) n \big]. \tag{14d}$$

Here, v denotes the membrane potential, m and h are the activation and inactivation of the sodium current, respectively, while n is the activation of the potassium current. Moreover, C is the capacitance, as before, and I denotes the current injected into the system. The other three

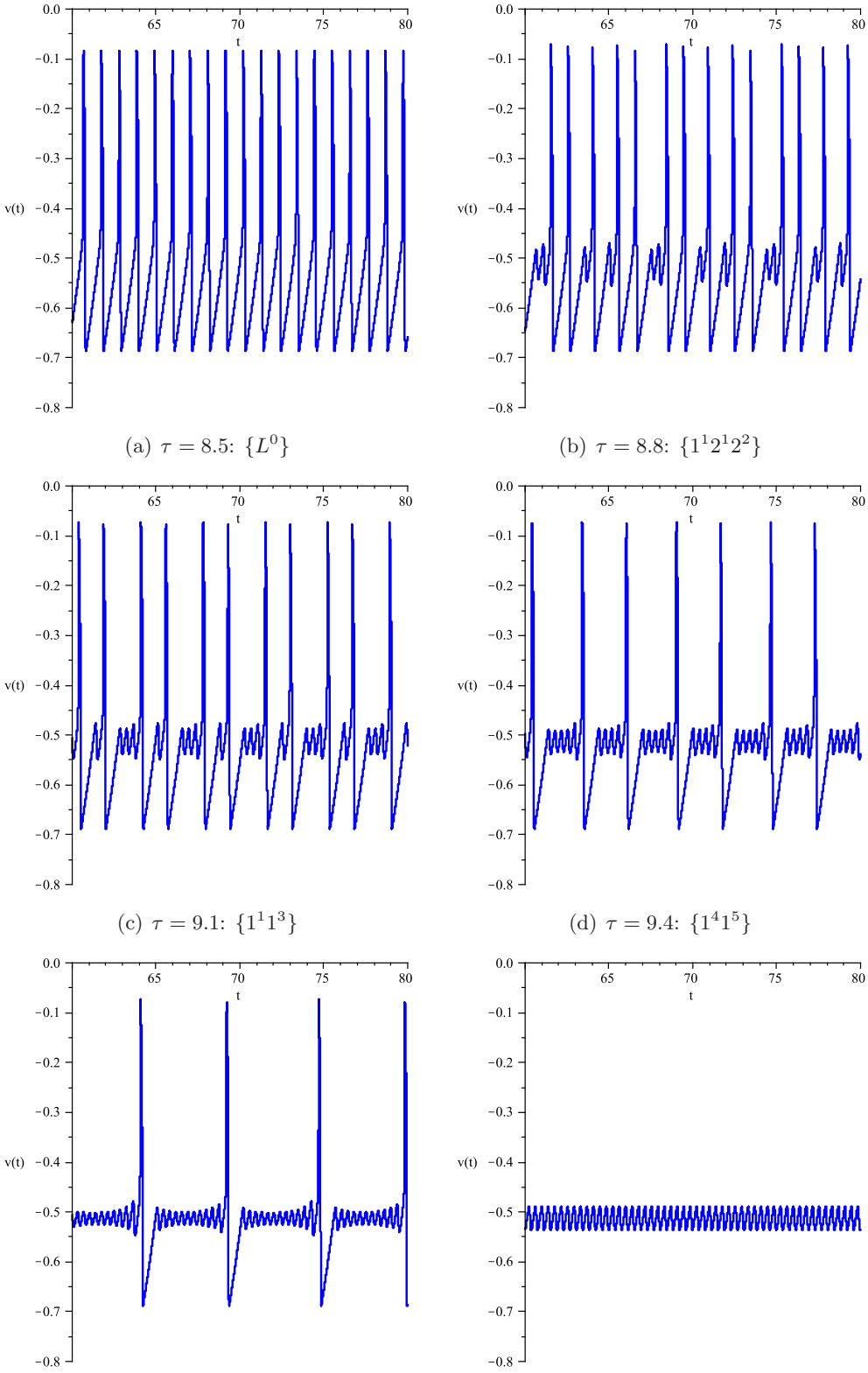

(a) $\tau = 8.5$: $\{L^0\}$

(b) $\tau = 8.8$: $\{1^1 2^1 2^2\}$

(c) $\tau = 9.1$: $\{1^1 1^3\}$

(d) $\tau = 9.4$: $\{1^4 1^5\}$

(e) $\tau = 9.7$: $\{1^{11} 1^{12}\}$

(f) $\tau = 10.0$: $\{0^k\}$

Figure 4. Mixed-mode dynamics in (13) upon variation of τ.

terms in (14a) represent ionic currents: a fast sodium current, a delayed potassium current and a leak current. The dynamics of the voltage-dependent gating variables m, h and n is governed by the right-hand sides in (14b), (14c) and (14d), respectively, with τ_m, τ_h and τ_n the time constants scaling the rates of change of these variables. We note that the classical Hodgkin-Huxley equations are recovered for $\tau_x = 1$ ($x = m, h, n$); indeed, the modification introduced in [8] referred precisely to the case where these constants are independent and not all equal. In particular, Doi *et al.* described a significant slowing of the firing rates in (14) if τ_h or τ_n are increased tenfold.

As was shown by Rubin and Wechselberger [38], a mere threefold increase in either parameter suffices to trigger the onset of irregular firing. For their analysis, they rewrite (14) as a non-dimensionalized system in standard form,

$$\varepsilon \dot{v} = I - m^3 h(v - E_{\mathrm{Na}}) - g_{\mathrm{K}} n^4 (v - E_{\mathrm{K}}) - g_\ell (v - E_\ell), \tag{15a}$$

$$\varepsilon \dot{m} = \frac{1}{\tau_m t_m(v)} [m_\infty(v) - m], \tag{15b}$$

$$\dot{h} = \frac{1}{\tau_h t_h(v)} [h_\infty(v) - h], \tag{15c}$$

$$\dot{n} = \frac{1}{\tau_n t_n(v)} [n_\infty(v) - v], \tag{15d}$$

where we have retained the notation from (14) for the sake of convenience. The equations in (15) are then studied under systematic variation of τ_h, τ_n and the applied current I. In particular, it is proved in [38] that a conventional reduction of (14) to a planar system, as suggested in [35], does not capture the full dynamics of the problem. Again, (15) is naturally a fast-slow system for ε sufficiently small.

However, while Rubin and Wechselberger [38, 39] group v and m as fast and h and n as slow to explain the generation of mixed-mode dynamics in (15) via a folded node singularity, h and n actually evolve on different scales if $\tau_h \neq \tau_n$: an increase in one of the two leads to a separation of the h- and n-dynamics, resulting in a three time-scale structure. Consequently, the critical value of I (which is the bifurcation parameter in this case) is significantly increased for physiologically realistic ε-values, as the theory developed in [43] breaks down away from the singular limit of $\varepsilon \to 0$; details can be found in [39] as well as in the upcoming article [21].

Representative time series of v upon variation of I are shown in Figure 5, with $\tau_m = 1$, $\tau_h = 3$ and $\tau_n = 1$ throughout. We again find a rich variety of complex mixed-mode patterns; note that more exotic patterns seem to be possible here than are observed in the previous example.

6. A canonical model, revisited

Both the simplified Wilson-Callaway model in (13) and the modified Hodgkin-Huxley equations in (15), though ostensibly four-dimensional, fit naturally into the context of the canonical three-dimensional three time-scale system (11). We restate that canonical model here for the reader's convenience,

$$\begin{aligned} x' &= -y + f_2 x^2 + f_3 x^3, \\ y' &= \varepsilon(x - z), \\ z' &= \varepsilon^2(\mu + \dots), \end{aligned}$$

where the prime now denotes differentiation with respect to the fast time $t = \frac{\tau}{\varepsilon}$. Taking into account that $v_1 \approx v_2$ for $d \gg 1$ in (13), i.e., that the voltage traces of the two compartments are virtually indistinguishable if the coupling is sufficiently strong, one can eliminate one of v_1 or v_2 via a center manifold reduction. Similarly, in the context of (15), it is well-known that $m \approx m_\infty$

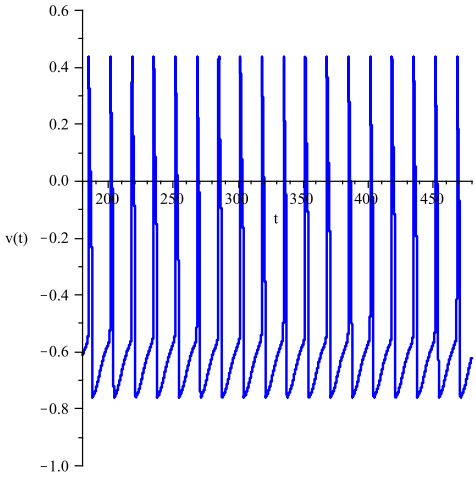

(a) $I = 9.6$: $\{L^0\}$

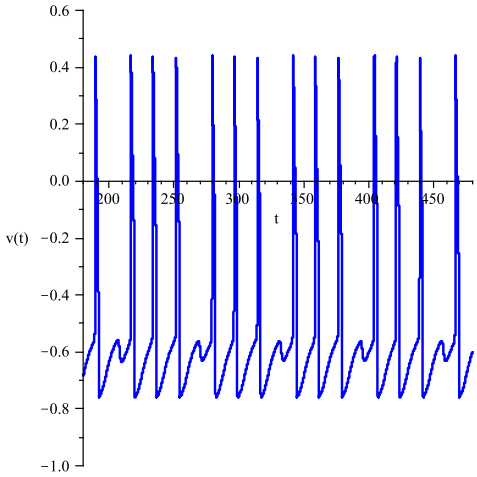

(b) $I = 9.3$: $\{3^1\}$

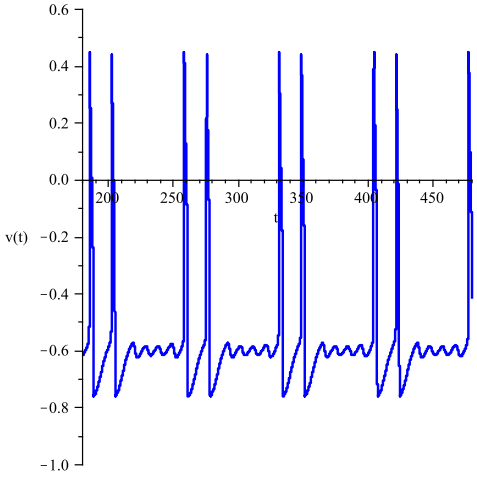

(c) $I = 9.0$: $\{2^4\}$

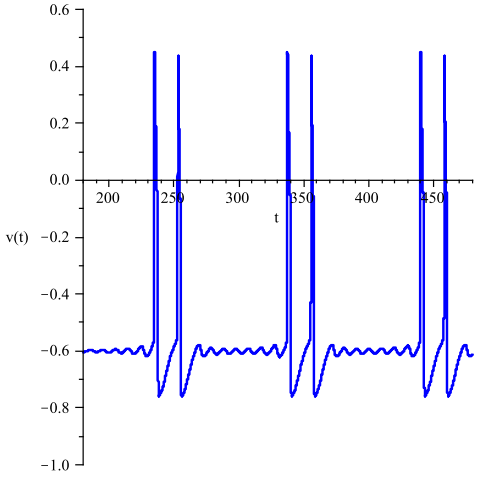

(d) $I = 8.7$: $\{2^7\}$

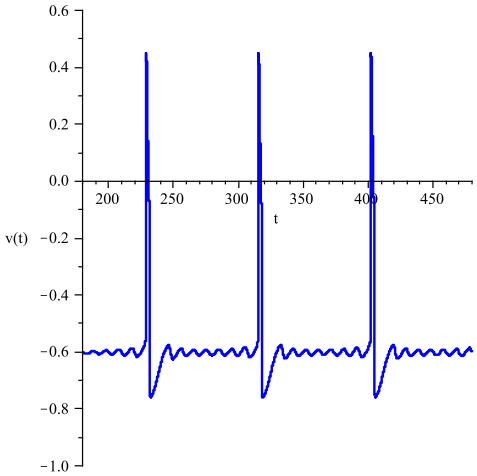

(e) $I = 8.4$: $\{1^7\}$

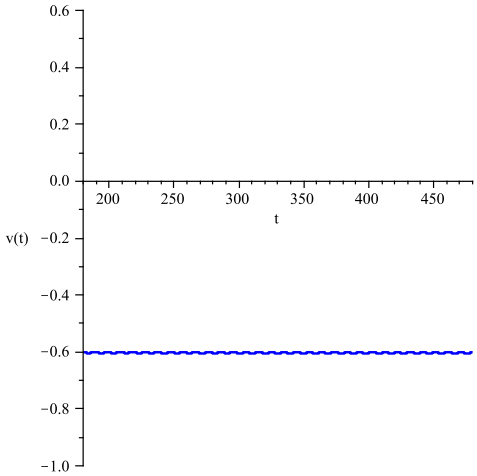

(f) $I = 8.1$: $\{0^k\}$

Figure 5. Mixed-mode dynamics in (15) upon variation of I.

gives a leading-order center manifold and, hence, that the m-equation can be eliminated from the system.

Without loss of generality, it thus suffices to understand the mixed-mode dynamics of the model system (11) in order to infer the corresponding dynamics of either (13) or (15). A treatment of how the equations in (13) fit into the framework of (11) can be found in [24], while the bifurcation structure of (15) as well as of the resulting mixed-mode dynamics will be fully elucidated in [21].

The canonical form in (11) was analyzed in detail in [23], where it was shown that the mixed-mode dynamics that is observed upon variation of μ is due to a 'slow passage through a canard explosion.' More precisely, the two-dimensional (x, y)-subsystem in (11) is in the standard form of a system that undergoes a classical two-dimensional canard explosion, with z corresponding to the canard parameter; recall the equations in (2). In our case, however, z is a dynamical parameter that varies on the slowest (ε^2-)time-scale in (11).

The dynamics of (11) is most easily understood by examining separately the local and the global aspects of the flow. We begin by discussing the local (canard) dynamics; then, we indicate how the global (relaxation) flow of (11) can be approximated. By combining these two ingredients of the dynamics, the local asymptotics close to the strong canard and the global return, we finally obtain an asymptotic description for the (global) return map that is induced by the flow of (11).

6.1. Local dynamics

To investigate the dynamics of (11) locally in a neighborhood of the fold curve ℓ^-, we define the rescaling

$$x = \sqrt{\varepsilon}\bar{x}, \quad y = \varepsilon\bar{y}, \quad z = \sqrt{\varepsilon}\bar{z}, \quad t = \frac{\bar{t}}{\sqrt{\varepsilon}}. \tag{16}$$

Substituting (16) into (11) and eliminating a factor of $\sqrt{\varepsilon}$ from the right-hand sides of the resulting equations, we find

$$\bar{x}' = -\bar{y} + f_2\bar{x}^2 + \sqrt{\varepsilon}f_3\bar{x}^3, \tag{17a}$$
$$\bar{y}' = \bar{x} - \bar{z}, \tag{17b}$$
$$\bar{z}' = \varepsilon(\mu + \dots). \tag{17c}$$

We note that the rescaling in (16) has removed the scale separation between x and y in (17), since both $\bar{x}$ and $\bar{y}$ now vary on an $\mathcal{O}(1)$-scale in $\bar{t}$, while $\bar{z}$ is still slow—$\mathcal{O}(\varepsilon)$ in $\bar{t}$. Moreover, the limiting system obtained for $\varepsilon = 0$ in (17),

$$\bar{x}' = -\bar{y} + f_2\bar{x}^2, \tag{18a}$$
$$\bar{y}' = \bar{x} - \bar{z}, \tag{18b}$$
$$\bar{z}' = 0, \tag{18c}$$

is integrable, with a constant of motion $H = H(\bar{x}, \bar{y})$ that can be found explicitly [23, 26]. The dynamics of (18) is well-understood, see e.g. [26]; for our purposes, it is important to note that the equations in (18) have a continuous family of periodic orbits which can be described by the level curves of H. We will denote these curves by $\{H = h\}$ here, with h a (real) parameter. In particular, the solution of (18) corresponding to $h = 0$ defines an invariant parabola in the $(\bar{x}, \bar{y})$-plane that acts as a separatrix between the closed level curves of H (for which $h > 0$) and the open ones (with $h < 0$); see Figure 6(a) for an illustration. Moreover, that parabola corresponds precisely to the strong canard in the singular limit of $\varepsilon \to 0$, in that its two branches give the continuation of $\mathcal{S}_0^{a-}$ and $\mathcal{S}_0^r$ into the fold region; see [23] for details.

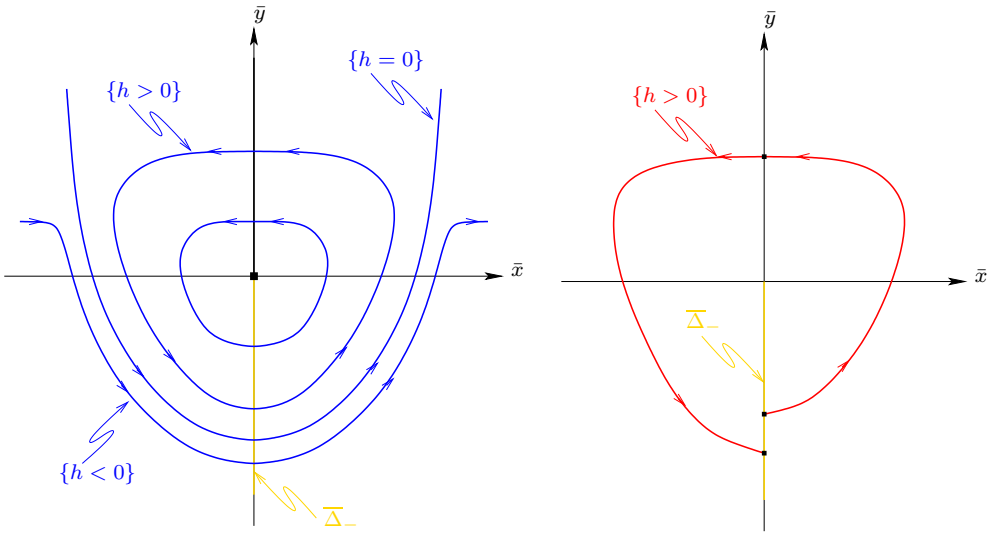

(a) $\varepsilon = 0$ (b) $\varepsilon > 0$

Figure 6. The level curves of H for (a) $\varepsilon = 0$ and (b) $\varepsilon > 0$.

Since the dynamics of the singular equations in (18) is integrable, we refer to the dynamics of the 'full,' perturbed system (17) as 'near-integrable.' That near-integrability of (17) allows us to study the resulting dynamics via a straightforward perturbation analysis: we are interested in the break-up, for $\varepsilon > 0$, of the singular orbits in (18) that correspond one-to-one to level curves $\{H = h\}$; see Figure 6(b). The asymptotic formulas describing that break-up in the rescaled $(\bar{x}, \bar{y}, \bar{z})$-variables are then used for approximating the flow of (17) near the fold: with Δ denoting the Poincaré section that bisects $\mathcal{S}_0$ across the fold at ℓ^- and $\Delta_- := \Delta\big|_{y<0}$, it can be shown that the return map $\overline{\Pi}$ for (17) is well-defined as a map from Δ_- to itself. A detailed study of the dynamics of system (17), including a proof, for ε sufficiently small, of the existence of the strong canard Γ^0_ε as well as of a family of bifurcating secondary canards $\{\Gamma^k_\varepsilon\}_{k\geq 1}$, can be found in [23].

***Remark* 1.** For a rigorous analysis of the local dynamics of (11) via blow-up, it is not sufficient to consider the 'rescaling' chart defined by the transformation in (16). Rather, one additionally has to account for the dynamics in two 'phase-directional' charts that cover the entry of solutions into the fold region and the exit from that region; see again [23] for details.

6.2. Global dynamics

We now briefly describe the global return mechanism that governs the dynamics of (11) outside the fold region once the local passage through a canard explosion has been completed. The corresponding argument in [23] relies entirely on standard geometric singular perturbation (Fenichel) theory [12, 19]. In particular, it suffices to restrict the analysis to the leading-order dynamics of (11), i.e., to the reduced problem on $\mathcal{S}_0$ given by

$$\begin{aligned} x' &= -(x - z), \\ z' &= -\varepsilon(\mu + \dots)\phi'(x), \end{aligned}$$

to obtain an approximation for the global return that is consistent to the order considered in our analysis; cf. also [23]. Solving these equations for $z(x)$, one finds

$$z(x) - z(x_0) = \varepsilon\mu \int_{x_0}^{x} \frac{\phi'(\xi)}{\xi}\, d\xi \tag{19}$$

to lowest order, where x_0 denotes a suitable initial x-value on $\mathcal{S}_0$. By evaluating the formula in (19) to account for the transition along both $\mathcal{S}_0^{a+}$ and $\mathcal{S}_0^r$ under the reduced dynamics of (11), one can derive asymptotic estimates for the global 'amount of return' of z after one relaxation cycle, as well as for the critical value of μ for which MMOs cease to exist in (11); we refer the reader to [23] for details.

6.3. Return map

The return map for system (11) is formulated by combining the results of the previous two subsections. It is intuitively clear that the local dynamics (as described in Section 6.1) is responsible for the small-amplitude (sub-threshold) component of the mixed-mode dynamics of (11). The global return mechanism, on the other hand, corresponds to the large-amplitude (relaxation) component of the time series; see Section 6.2. To understand how a particular pattern is generated by the interplay of these two aspects of the dynamics, recall the definition of the Poincaré section Δ, and let $\mathcal{C}_\varepsilon^-$ and $\mathcal{C}_\varepsilon^+$ be defined as the intersection curves of the slow manifold $\mathcal{S}_\varepsilon$ (or, rather, of its extension into the fold region) with the section Δ. Moreover, recall the parameter h introduced in Section 6.1, as well as the fact that $h > 0$ and $h < 0$ correspond to closed and open level curves of H, respectively. Now, note that the dynamics of (11) is clearly h-dependent: if the h-value of an orbit crossing Δ is positive, its point of intersection with Δ lies 'above' $\mathcal{C}_\varepsilon^+$, and the return to Δ is described by the 'local' map $\overline{\Pi}$ in that case. Thus, the corresponding solution curve must stay in the fold region and undergo another small oscillation. If, on the other hand, that h-value is negative, the orbit intersects Δ 'below' $\mathcal{C}_\varepsilon^+$ in Δ, which implies that the solution must leave the fold region and exit into relaxation ('jump').

An iteration of this mechanism yields the sought-after return map on Δ, which we denote by Π; in particular, the fact that the sign of h can change after each iteration allows for a transition from the sub-threshold regime to large-scale relaxation, and vice versa. See Figure 7(a) for a schematic illustration of how a typical mixed-mode segment—1^2 in our case, cf. Figure 7(b)—is generated by Π.

6.4. Reduced return map

In a second step, the two-dimensional map Π (which is a function of both y and z) is reduced to a one-dimensional map Φ that is defined on a family of z-intervals corresponding to the so-called *sectors of rotation*; to be precise, the kth sector RS^k is given by a z-subinterval of $\mathcal{C}_\varepsilon^-$ that is bounded by the z-values associated with the $(k-1)$th and the kth secondary canard Γ_ε^{k-1} and Γ_ε^k, respectively. Trajectories passing through RS^k undergo k sub-threshold oscillations before exiting the fold region and entering relaxation. Therefore, the restriction of the 'reduced' map Φ to the kth sector can be regarded as a description of the recurrent dynamics on that sector, in the sense that stable fixed points of Φ on RS^k correspond to stable periodic time series with Farey sequence $\{1^k\}$. In general, the Farey sequence of a given mixed-mode trajectory is completely determined by the succession of sectors of rotation it visits; hence, the question which Farey seqences are admissible in (11) is intimately related to the width of these sectors, as well as to the contractive (or expansive) properties of the flow induced by Φ. See Figure 8 for a qualitative illustration of the graph of the reduced map Φ: although Φ is multimodal and (possibly) discontinuous at the boundaries of RS^k, it is one-dimensional and can hence be analyzed using the well-developed theory for one-dimensional maps; details can be found in [23].

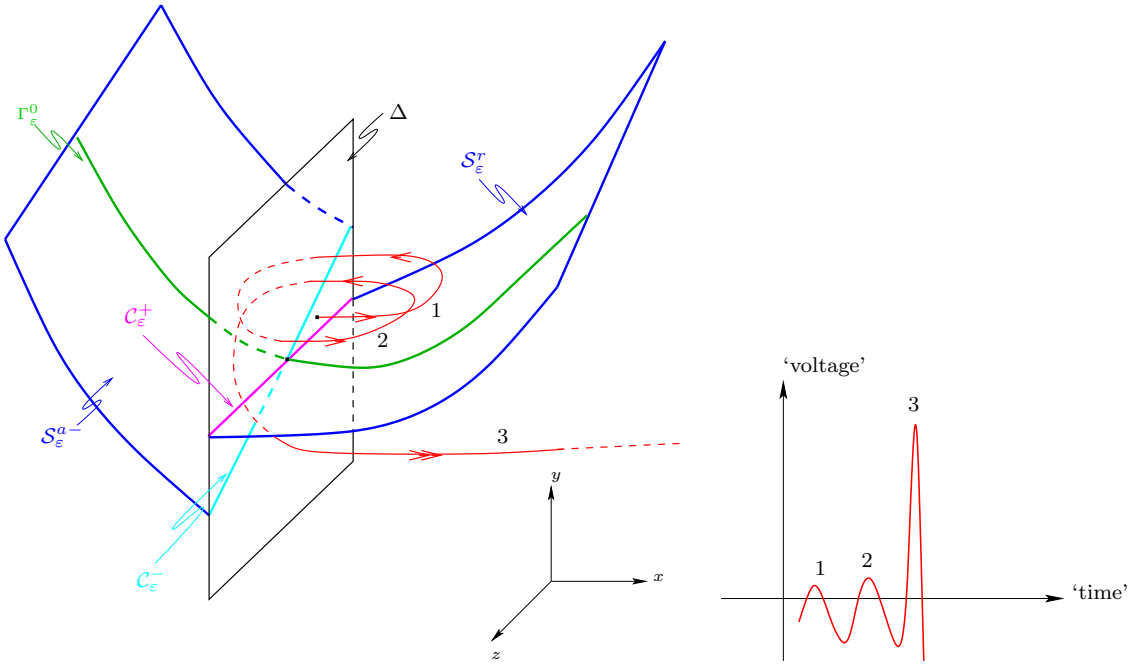

(a) Iteration of Π ... (b) ... generates the segment 1^2

Figure 7. The return map Π.

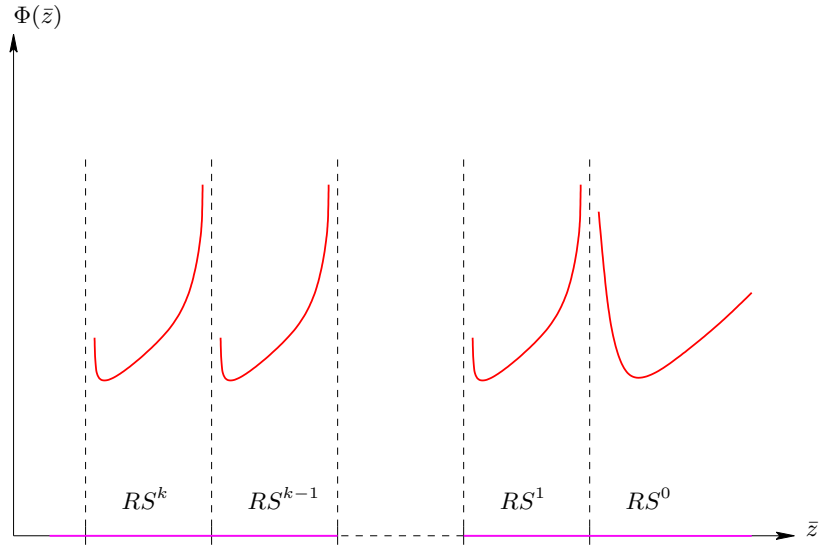

Figure 8. The reduced return map Φ.

Finally, we remark that the reduction of Π to Φ is exponentially accurate, in the sense that the resulting approximation error is exponentially small in ε. (It is important to note, however, that Φ is defined on a family of intervals, whereas the dynamics of (11) cannot be reduced accurately to that of a one-dimensional interval map, as is frequently postulated; see e.g. [31].)

7. Conclusions and discussion

In this article, which is mostly based on the ongoing work of Krupa and Wechselberger [27, 43], as well as of Krupa and Popović [21], we gave a brief overview of the generalized canard mechanism that can explain how mixed-mode dynamics arises in three-dimensional singularly perturbed systems of ordinary differential equations. Then, we presented a canonical form for one specific class of systems in which the dynamics evolves on three time-scales (fast, slow and super-slow), recall (11). That class is characterized by the leading-order terms in the relevant equations and corresponds to a 'folded saddle-node of type II with weak global return'; cf. the classification of Section 2. Here, the difference from the classical folded saddle-node scenario is that not only μ in (11c) is $\mathcal{O}(1)$, but that the higher-order terms are, too. The resulting weakness of the global return gives rise to the three time-scale structure in (11), which also explains why no slow passage through a Hopf bifurcation is observed, contrary to the case of a folded saddle-node (of type II) [27].

Although the equations in (11) are not covered by the existing standard theory of singularly perturbed systems, which accounts only for the presence of two time-scales, it was shown in [23] that the near-integrable nature of the dynamics of (11) still allows for a reasonably explicit analysis. Our approach there relied on a combination of local and global techniques—'blow-up,' or geometric desingularization [9, 25] and geometric singular perturbation (Fenichel) theory [12, 19], respectively—which allowed us to deduce a fairly complete picture of the global dynamics of (11). In particular, we were able to describe the bifurcation structure of the family of secondary canards $\{\Gamma_\varepsilon^k\}$ in considerable detail, obtaining precise asymptotic estimates for the size of the corresponding sectors of rotation $\{RS^k\}$ as well as for the relevant μ-intervals. These estimates, in turn, enabled us to draw detailed conclusions on the resulting mixed-mode dynamics in (11), both qualitatively and quantitatively. (It is, however, important to note that a full geometric analysis of the general folded saddle-node singularity is significantly more complicated, see the upcoming article [27].)

Our main results on the dynamics of (11), as obtained in [23], can be summarized as follows:

(i) As μ varies, one observes the unfolding of a full family of MMOs: small-amplitude regime $\{0^k\} \longrightarrow$ 'mixed' sequences $\{L_j^{k_j}\}$ (L_j large excursions, k_j small oscillations) $\longrightarrow$ relaxation regime $\{L^0\}$;

(ii) the width of the relevant μ-intervals is $\mathcal{O}(\varepsilon^\alpha)$ (in contrast to the two-dimensional case, where those intervals are exponentially small in ε), corresponding to a relatively robust canard phenomenon;

(iii) the resulting $\{L_j^{k_j}\}$-type mixed-mode dynamics is fairly regular:

  (a) the segments 1^k and 1^k1^{k-1} (one large excursion, $k \geq 1$ small oscillations) dominate;
  (b) the segment L^1 (L large excursions, one small oscillation) is possible for $L \geq 1$;
  (c) the segment L^k ($L \geq 2$ large excursions, $k \geq 2$ small oscillations) is rare.

We then presented two examples of problems that can be subsumed into the framework of the canonical form given by (11), the Wilson-Callaway model [44, 31] for the dynamics of the dopaminergic neuron in rats and a modification of the classical Hodgkin-Huxley equations [17, 8] for the squid giant axon. (In fact, it was the simplified version of the Wilson-Callaway equations analyzed in [31] that motivated us to formulate (11).) The corresponding analysis can be found in [24] and in the upcoming article [21], respectively; interestingly, the mixed-mode dynamics observed in the modified Hodgkin-Huxley model seems to allow for a larger variety of exotic mixed-mode patterns than is predicted in item (iii) above, cf. also [39]. This discrepancy is probably due to differences in the specific global return in (10), as compared to the generic form that is assumed in (11c). The precise bifurcation structure of (10) will depend strongly on the properties of that return mechanism; the interplay of μ and the higher-order terms in (11c)

determines in particular how far 'back' z can be reset during the global return phase. The more substantial that reset, the larger the number of sectors of rotation a mixed-mode trajectory can visit, which in turn translates into a potentially higher prevalence of mixed $\{L_j^{k_j}\}$-type orbits.

Our results on the dynamics of (11) are in stark contrast to those obtained in the case of a folded node [4, 43], which seems to be the only other realization of the generalized canard mechanism for which a comparable analysis is available: due to the strong contraction during the initial phase of a local passage of node type, the resulting mixed-mode dynamics is regular and robust, in the sense that no stable irregular mixed-mode patterns are possible. Rather, periodic 1^k-type dynamics (as in item (iii)(a) above) is stable for most μ-values, see [23] for details.

The analysis in [23], in combination with the results obtained by Wechselberger [43] as well as by Brøns, Krupa and Wechselberger [4], thus represents a first step towards creating a potentially unifying framework for the classification of the mixed-mode dynamics observed in a variety of applicational problems, at least in cases where the underlying dynamics varies on multiple scales. (In that context, we conjecture that the generalized canard mechanism might underlie several of the other known MMO mechanisms.) The long-term goal is to develop a more complete classification of the canard phenomena that can occur in three dimensions, resulting in a 'modular toolbox' of prototypical systems. Such a toolbox could be particularly helpful in finding 'minimal' models in applications when combined with dimension reduction techniques [4, 22]. These and similar topics are the subject of ongoing research.

Acknowledgments
N. Popović is grateful to his wife Heidi for her critical reading of the original manuscript, as well as for many helpful suggestions.

References

[1] Benoît E 1983 *Astérisque* **109** 159
[2] Bold K, Edwards C, Guckenheimer J, Guharay S, Hoffman K, Hubbard J, Oliva R and Weckesser W 2003 *SIAM J. Appl. Dyn. Syst.* **2** 570
[3] Benoît E, Callot J-L, Diener F and Diener M 1981 *Collect. Math.* **32** 37
[4] Brøns M, Krupa M and Wechselberger M 2006 *Fields Inst. Commun.* **49** 36
[5] Diener M 1984 *Math. Intelligencer* **6** 38
[6] Desroches M, Krauskopf B and Osinga H M 2007 The geometry of slow manifolds near a folded node *Preprint*
[7] Desroches M, Krauskopf B and Osinga H M 2008 *Chaos* **18** 015107
[8] Doi S, Nabetani S and Kumagai S 2001 *Biol. Cybern.* **85** 51
[9] Dumortier F and Roussarie R 1996 *Mem. Amer. Math. Soc.* **121**
[10] Eckhaus W 1983 *Relaxation oscillations including a standard chase on French ducks* (Asymptotic Analysis II, Lecture Notes in Math. vol 985) (New York: Springer-Verlag) p 449
[11] Epstein I R and Showalter K 1996 *J. Phys. Chem.* **100** 13132
[12] Fenichel N 1979 *J. Differential Equations* **31** 53
[13] Guckenheimer J 2008 Singular Hopf bifurcation in systems with two slow variables *Preprint*
[14] Guckenheimer J and Haiduc R 2005 *Mosc. Math. J.* **5** 91
[15] Guckenheimer J, Harris-Warwick R, Peck J and Wilms A 1997 *J. Comput. Neurosci.* **4** 255
[16] Guckenheimer J and Wilms A 2000 *Phys. D* **139** 196
[17] Hodgkin A L and Huxley A F 1952 *J. Physiol. (London)* **117** 500
[18] Hardy G H and Wright E M 1979 *An Introduction to the Theory of Numbers* (Fifth edition) (New York: The Clarendon Press, Oxford University Press)
[19] Jones C K R T 1995 *Geometric singular perturbation theory* (Dynamical Systems, Lecture Notes in Math. vol 1609) (New York: Springer-Verlag) p 44
[20] Koper M T M 1995 *Phys. D* **80** 72
[21] Krupa M and Popović N 2008 Mixed-mode oscillations in a modified Hodgkin-Huxley model: a three time-scale approach *In preparation*
[22] Krupa M and Popović N 2008 Canards in systems with more than two slow variables *In preparation*
[23] Krupa M, Popović N and Kopell N 2008 *SIAM J. Appl. Dyn. Syst.* **7** 361

[24] Krupa M, Popović N, Kopell N and Rotstein H G 2008 *Chaos* **18** 015106
[25] Krupa M and Szmolyan P 2001 *SIAM J. Math. Anal.* **33** 286
[26] Krupa M and Szmolyan P 2001 *J. Differential Equations* **174** 312
[27] Krupa M and Wechselberger M 2008 Local analysis near a folded saddle-node singularity *Preprint*
[28] Larter R and Steinmetz C G 1991 *Philos. Trans. Roy. Soc. London Ser. A* **337** 291
[29] Larter R, Steinmetz C G and Aguda B D 1988 *J. Phys. Chem.* **89** 6506
[30] Moehlis J 2002 *J. Nonlin. Sci.* **12** 319
[31] Medvedev G S and Cisternas J E 2004 *Phys. D* **194** 333
[32] Mishchenko E F, Kolesov Yu S, Kolesov A Yu and Rhozov N Kh 1994 *Asymptotic Methods in Singularly Perturbed Systems* (Monogr. Contemp. Math.) (New York: Consultants Bureau)
[33] Milik A, Szmolyan P, Löffelmann H and Gröller E 1998 *Internat. J. Bifur. Chaos Appl. Sci. Engrg.* **8** 505
[34] Petrov V, Scott S K and Showalter K 1992 *J. Chem. Phys.* **97** 6191
[35] Rinzel J 1985 *Federation Proc.* **44** 2944
[36] Rotstein H G and Kuske R 2006 *Phys. D* **215** 46
[37] Rotstein H G, Oppermann T, White J A and Kopell N 2006 *J. Comput. Neurosci.* **21** 271
[38] Rubin J and Wechselberger M 2007 *Biol. Cybernet.* **97** 5
[39] Rubin J and Wechselberger M 2008 *Chaos* **18** 015105
[40] Sobolev V A and Shchepakina E A 1997 *Differential Equations* **32** 1177
[41] Smzolyan P and Wechselberger M 2001 *J. Differential Equations* **177** 419
[42] Szmolyan P and Wechselberger M 2004 *J. Differential Equations* **200** 69
[43] Wechselberger M 2005 *SIAM J. Appl. Dyn. Syst.* **4** 101
[44] Wilson C J and Calloway J C 2000 *J. Neurophysiol.* **83** 3084
[45] Zhabotinsky A M 1964 *Biofizika* **9** 306